J. Fluid Mech. (2005), *vol.* 524, *pp.* 121–130. © 2005 Cambridge University Press
DOI: 10.1017/S0022112004002411 Printed in the United Kingdom

Bursting thin liquid films

By N. BREMOND† AND E. VILLERMAUX‡

IRPHE, Université de Provence, Aix-Marseille 1, Technopôle de Château-Gombert, 49, rue Frédéric Joliot-Curie 13384 Marseille Cedex 13, France

(Received 16 February 2004 and in revised form 7 October 2004)

The breakup of a free thin liquid film subjected to an impulsive acceleration is investigated. A soap film is stretched on a frame at the exit of a shock tube. As the shock impacts the film, the film accelerates within a very short time and detaches from the frame at a constant velocity function of the shock strength. The liquid thickness modulations amplify and eventually the film is perforated with a number of holes, subsequently growing in radius and connecting to each other. The initially connex film is left in the form of a web of liquid ligaments which break into droplets. Both the hole density and formation time depend on the film velocity. We analyse these observations with an impulsive Rayleigh–Taylor instability incorporating liquid surface tension. It is shown to account for both the mode selection and its associated time of growth, providing a criterion for the film bursting time and hole density.

1. Introduction

Rayleigh (1883) was the first to analyse the stability of a density interface between two superposed semi-infinite media subjected to a constant acceleration normal to the interface. Taylor (1950) then investigated the stability of a fluid layer of a given density sandwiched between two fluids of a different density. They concluded that these situations are always unstable with, since surface tension was not taken into account in both of these studies, the same dispersion equation. The growth rate depends solely on the density contrast between the phases, the acceleration and the wavenumber. If the density transition is sharp at the interface, there is no mode selection. In particular, the instability growth rate is independent of the layer thickness in the case studied by Taylor, and Rayleigh shows how a continuous transition of the density over a finite thickness at the interface results in a saturation of the growth rate at large wavenumber only. Surface tension does induce mode selection on the capillary lengthscale, as shown in Chandrasekhar (1961).

Soon after the works of Taylor (1950) and Lewis (1950), Keller & Kolodner (1954) extended Taylor's analysis to incorporate surface tension. Although not discussed in detail by these authors, a new phenomenon arises in that case from the coupling between the two interfaces of the layer which, when the layer is much thinner than the capillary length, induces a considerable slowing down of the amplification rate and a shift of the selected mode towards larger lengthscales (figure 1*b*). We first recall the main results of this 'thin layer limit' before discussing how it can be explored experimentally.

A liquid sheet of uniform thickness h is sandwiched between two infinite gas phases and is subjected to a constant acceleration a perpendicular to its surfaces (see e.g.

† Present address: Department of Applied Physics, University of Twente, 7500 AE Enschede, The Netherlands.

‡ Also at: Institut Universitaire de France.

https://doi.org/10.1017/S0022112004002411 Published online by Cambridge University Press

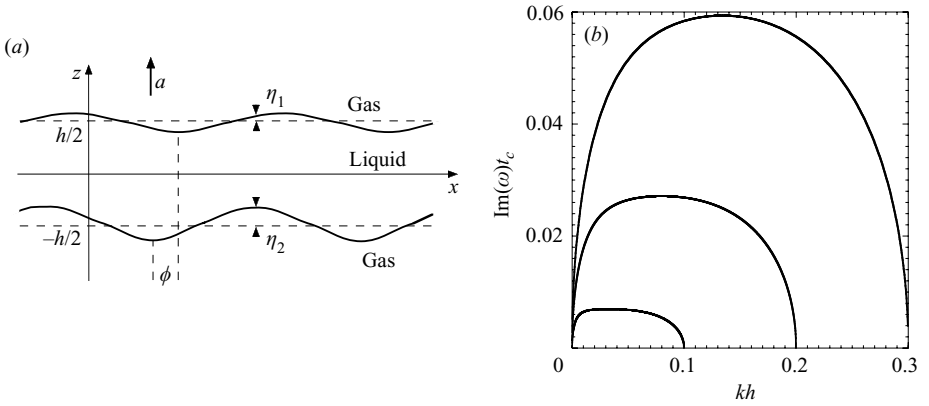


FIGURE 1. (*a*) Sketch of the destabilization of a liquid sheet when accelerated in a direction perpendicular to its surfaces. (*b*) Dispersion relation (1.1) for three different critical wavenumbers, $\tilde{k}_c = 0.1$, 0.2 and 0.3.

figure 1*a*). The initial modulations of the interface positions are proportional to the Fourier modes $\eta_1 = \eta_{01}\exp(\mathrm{i}kx - \mathrm{i}\omega t)$ for the upper interface and $\eta_2 = \eta_{02}\exp(\mathrm{i}kx - \mathrm{i}\omega t + \mathrm{i}\phi)$ for the lower. The initial amplitudes η_{01} and η_{02} are positive real, and the phase shift ϕ is *a priori* free. Lengths and time are made non-dimensional by h and $t_c = \sqrt{\rho h^3/\sigma}$, the capillary time based on the liquid density and surface tension, respectively. Neglecting the density of the gas phase in front of the liquid, the inviscid, dimensionless (with tilde variables) dispersion equation is (Keller & Kolodner 1954)

$$\tilde{\omega}^2 = \tilde{k}^3 \coth(\tilde{k})\left\{1 \pm [1 - (1 - (\tilde{k}_c/\tilde{k})^4)\tanh^2(\tilde{k})]^{1/2}\right\}, \tag{1.1}$$

where $\tilde{k}_c = \sqrt{\rho a h^2/\sigma}$ is the capillary wavenumber. Equation (1.1) with the minus sign presents an unstable range of wavenumbers for $0 < k < k_c$ where the shape of the amplification factor $\mathrm{Im}\{\tilde{\omega}\} = \tilde{\omega}_{\mathrm{im}}$ depends on $\tilde{k}_c$ (figure 1*b*). The dispersion relation coincides with that of the peristaltic mode $\tilde{\omega} = \tilde{k}^2/\sqrt{2}$ of free films for $k_c \to 0$ in that case. However, the initial amplitudes and phase of the amplified perturbations are linked by $\eta_{01}/\eta_{02} \sim (1 - \tilde{k})\cos(\phi)$. There is, in contrast with free films, no discrete phase selection in this problem.

When $\tilde{k}_c \gg 1$ (i.e. thick layer, large acceleration), one recovers the classical dispersion relation characteristic of an infinite medium $\tilde{\omega}^2 = \tilde{k}^3\{1 - (\tilde{k}_c/\tilde{k})^2\}$. The maximum growth rate $\omega_{\mathrm{im}} \sim (\rho a^3/\sigma)^{1/4}$ and the selected wavenumber $k_{\mathrm{m}} = k_c/\sqrt{3} \sim \sqrt{\rho a/\sigma}$ are independent of h.

When $\tilde{k}_c \ll 1$ (i.e. thin layer, weak acceleration), the dispersion relation 1.1 flattens and shrinks in the $\{\tilde{\omega}, \tilde{k}\}$-plane. In this limit, when $\tilde{k}$ is of order $\tilde{k}_c$, one has $\tilde{\omega}^2 = \tilde{k}^4/2\{1 - (\tilde{k}_c/\tilde{k})^4\}$, and when $\tilde{k} \to 0$ one has $\tilde{\omega}^2 = -\tilde{k}_c^2\tilde{k}$. The wavenumber which connects these two extremes $k_{\mathrm{p}} = k_c^2 h/2$ defines the inner border of a plateau whose associated growth rate is $\omega_{\mathrm{im}} \sim (\rho a^2 h/\sigma)^{1/2}$. Close to this border is the most amplified wavenumber $k_{\mathrm{m}} = 6^{-1/6} k_c^{4/3} h^{1/3}$ (which results from the maximization of $\tilde{\omega}^2 = \tilde{k}^4/2 - \tilde{k}_c^4/2 + \tilde{k}_c^8/8\tilde{k}^2$, valid for $\tilde{k}_c \to 0$ and $\tilde{k} \to 0$). Both k_{m} and ω_{im} go to zero for a vanishingly thin layer. This is why gently blowing on a soap film does not break it: then the film undergoes a very slow destabilization. A strong acceleration imparted to the film does, however, lead to its destabilization. This is realized by imposing a pressure difference between the two sides of a soap film stretched on a frame positioned at the exit of a shock tube. The film accelerates violently within a short time on the passage of the shock, giving it an impulsive acceleration of the type studied by Markstein (1957),

https://doi.org/10.1017/S0022112004002411 Published online by Cambridge University Press

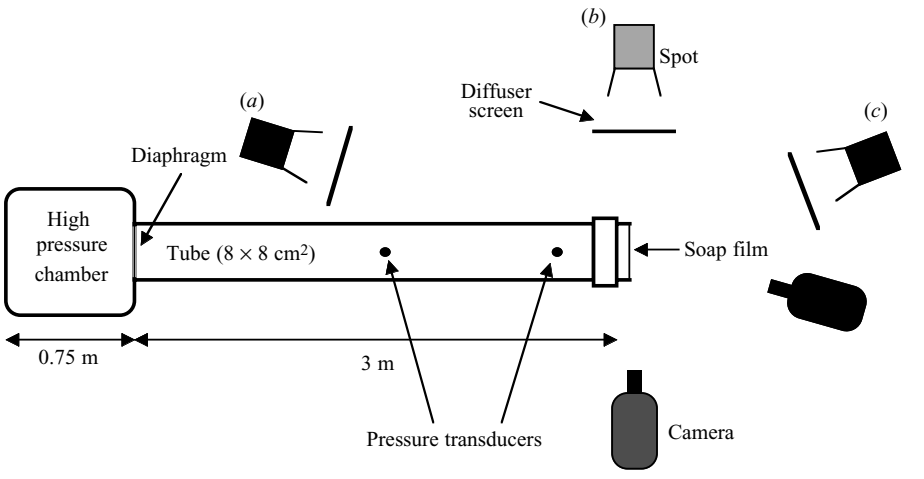


FIGURE 2. Set-up showing the different views and illumination procedures, (*a*) front view and back lighting, (*b*) side view and back lighting, (*c*) front view and lighting by reflection.

Richtmyer (1960), Meshkov (1969) and more recently by Rightley, Vorobieff & Benjamin (1997) and Niederhaus & Jacobs (2003) for gases or miscible liquids. The present study involving liquid–gas interfaces presents a natural (i.e. not solely induced by the initial conditions) mode selection mechanism owing to the involvement of surface tension.

2. Experimental set-up

Experiments were performed in a 3 m long shock tube with a $8 \times 8\,\mathrm{cm}^2$ square section (figure 2). A high pressure chamber is connected to the tube by an aluminium diaphragm. The thickness of the diaphragm sets its rupture pressure and so the shock strength. The use of one or several layers of 12 μm thick aluminium paper allowed the shock Mach numbers $M = u_c/u_s$ to be varied from 1.03 to 1.21. The velocity of the shock wave u_c is measured by the delay between the signals of two pressure transducers and the sound velocity u_s is determined at atmospheric pressure and ambient temperature. The liquid film is stretched on a square frame from a solution of water plus glycerol (10% in volume) and an industrial detergent below the critical miscellar concentration. The frame is then fixed at the exit of the open shock tube. The surface tension of the solution is measured by stalactometry and is $0.03\,\mathrm{kg\,s}^{-2}$. Since the frame is placed vertically, it drains under the action of gravity, producing a thickness field slowly thickening downwards in time. The thickness field was measured at a given time by pinching a hole in the film and following the recession of the rim position by capillary forces (Taylor 1959; Culick 1960; Keller 1983). The thickness varies from 1.7 to 2.7 μm on the 4 cm high visualization window. The dynamics of the film on the passage of the shock was recorded by a Phantom v6 high-speed video camera. The light source is a HMI projector (LTM of 575 W) which could be operated either in transmission through the film, or by reflection.

3. Observations and results

3.1. *Film velocity*

Figure 3 shows a side view of the soap film at different instants of time after it has interacted with the shock. The film is initially weakly curved because the diaphragm

https://doi.org/10.1017/S0022112004002411 Published online by Cambridge University Press

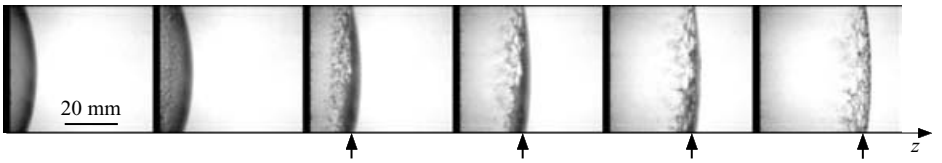


FIGURE 3. Side views of the soap film position (marked by an arrow) on the passage of the shock wave, $M = 1.07$. Time increases from left to right by steps of $\Delta t = 0.2$ ms.

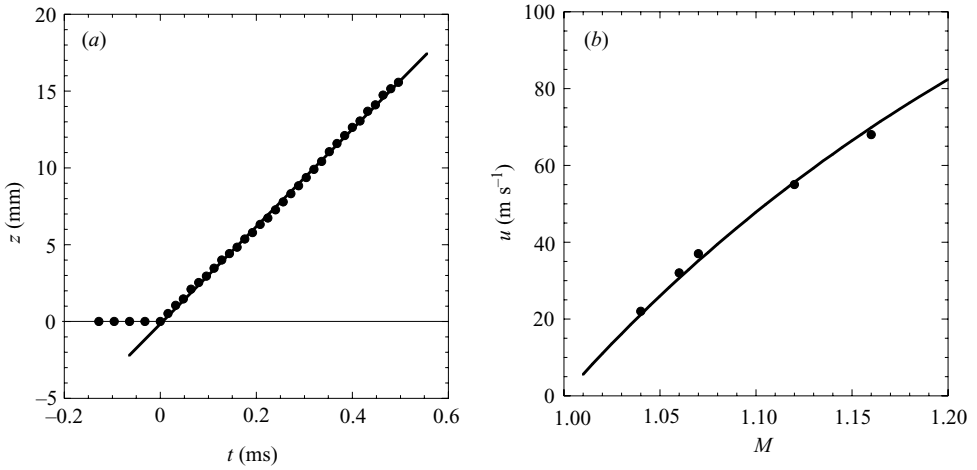


FIGURE 4. (*a*) Trajectory of the film, $M = 1.06$. (*b*) Dependence of the experimental film velocity on M (●) and terminal velocity u predicted in (3.1) (—).

inflates somewhat before breaking, therefore slightly displacing the air in the tube. After the passage of the shock, the film is torn off the frame and moves in the direction of the shock propagation at constant velocity (figure 4*a*). The film has reached its constant velocity within a time period shorter than the inverse of the camera sampling rate, 1.6×10^{-5} s. This time is, as will be seen below, much smaller than the time of the film instability growth.

The liquid film is pushed forward when the shock impacts it. The relation between the pressure P_1 behind the wave front and the pressure P_0 of the air initially at rest in front of the shock is $P_1/P_0 = (2\gamma M^2 - \gamma + 1)/(\gamma + 1)$ (Landau & Lifchitz 1989). Since the acoustic impedance of water is much larger than that of air, the shock is nearly completely reflected at the liquid surface (Henderson 1989) and the pressure P_2 behind the reflected wave is then $P_2 = 2P_1 - P_0$. As the film moves, it forms a compression wave in front of it of pressure P_4, and a rarefaction wave behind it of pressure P_3. While the film velocity $U(t)$ remains much smaller than the sound speed in air u_s (which is, by far, the case here), these pressures are $P_3 \approx P_2(1 - \gamma U(t)/u_s)$ and $P_4 \approx P_0(1 + \gamma U(t)/u_s)$. The film velocity $U(t)$ follows from momentum conservation $\rho h \mathrm{d}U(t)/\mathrm{d}t = P_3 - P_4$:

$$U(t) = u\left(1 - \frac{\mathrm{e}^{-t/\tau}}{2(M^2 - 1)}\right) \tag{3.1}$$

where $\tau = \rho h u_s(\gamma + 1)/P_0\gamma(2\gamma M^2 - \gamma + 1)$ is the characteristic time for the film to reach the final velocity $u = u_s 2(M^2 - 1)/(2\gamma M^2 - \gamma + 1)$ (figure 4*b*). The inertia of the

https://doi.org/10.1017/S0022112004002411 Published online by Cambridge University Press

liquid only appears in the transient, and the final velocity is solely determined by the shock strength and the compressibility properties of the gas. For the present conditions ($\gamma = 1.4$, $P_0 = 10^5$ Pa, $u_s = 340\,\mathrm{m\,s^{-1}}$, $h = 2\,\mu$m), τ is smaller than 10^{-5} s.

3.2. *Instability development*

Figure 5(*a*) shows bursting sequences for three different Mach numbers when the film is illuminated from behind. The film is perforated by holes which, once formed, expand by capillary recession and then merge, leaving the initially connex liquid film in the form of a web of liquid ligaments which subsequently break into droplets. The number of holes $n(t)$ increases in time, then saturates and reaches a maximum N before decreasing because of the mutual interaction between the holes which annihilate when they merge. Both the hole density and the perforation rate are an increasing function of the Mach number, as can be seen on figure 5(*b*). The rate of increase of the hole number $n(t)$ defines a characteristic formation time t_n as the inverse of the perforation rate before saturation, shown on figure 6(*b*). This back lighting configuration does not permit determination of the instant of interaction of the shock with the film and therefore the curves on figure 5(*b*) have different origins of time. Observation of the same sequence of events by light reflection (figure 6*a*) allows determination of the time of impact of the film by the shock wave. The origin of time is determined when the reflected image of the light source on the film is first deformed. From this second set of experiments, we extract the time of the first film perforation t_1. This time is larger than the inverse of the perforation rate t_n by two orders of magnitude and decreases more slowly with M, as can be seen on figure 6(*b*).

4. Film dynamics and bursting

Before reaching a constant velocity, the film is accelerated during a time period smaller by two to three orders of magnitude than its destabilization period (figures 4 and 5). After the shock has hit the film surface, the pressure wave propagates across the liquid width at the sound speed $u_{s\ell}$ and travels between the two interfaces in a time given by $h/u_{s\ell} \approx 2\times10^{-6}/1500 \sim 10^{-9}$ s, much smaller than the time needed for the film to reach a constant translation velocity u, which is of order $\tau \approx 10^{-5}$ s, itself much smaller that the development time of the instability, of order 10^{-3} s. The time during which the impulse is communicated to the film is thus very short compared to the instability time, but also very short compared to the acceleration time of the film. When describing the dynamics of the perturbations, it is therefore legitimate to assume a piecewise constant acceleration, and use Keller & Kolodner dispersion relation (1.1) with $a(t)$ suitably adapted in each of the time intervals as

$$a(t) = u\Delta(t) \tag{4.1}$$

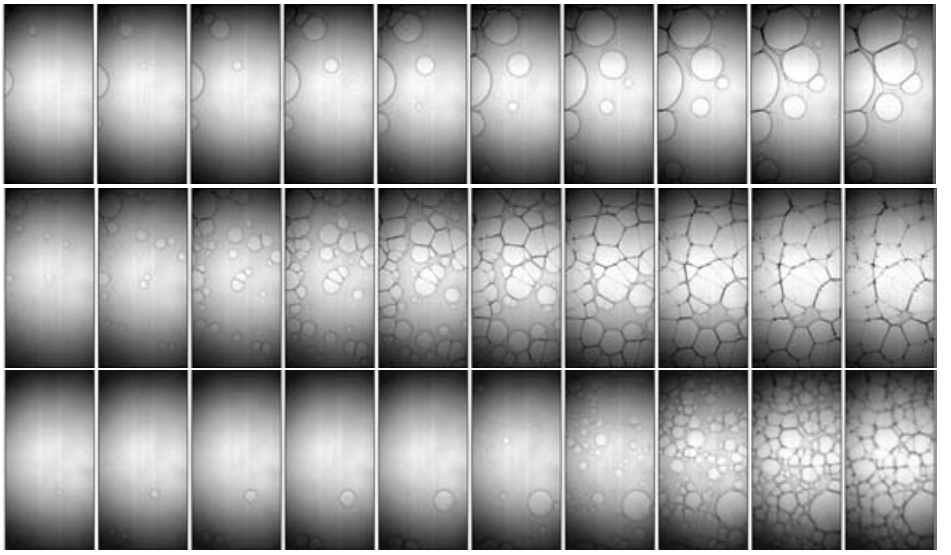
where $\Delta(t)$ is a step function equal to $1/\tau$ for $t < \tau$ and equal to 0 for $t > \tau$. We write the thickness modulation $\tilde{\eta}$ as

$$\tilde{\eta}(\tilde{x}, \tilde{t}) = \tilde{\eta}_0 f(\tilde{t})\, \mathrm{e}^{\mathrm{i}\tilde{k}\tilde{x}} \tag{4.2}$$

with the initial conditions for the shape function $f(t)$

$$f(\tilde{t} = 0) = 1 \qquad \text{and} \qquad \frac{\mathrm{d}f}{\mathrm{d}\tilde{t}}(\tilde{t} = 0) = 0. \tag{4.3}$$

https://doi.org/10.1017/S0022112004002411 Published online by Cambridge University Press



(*a*)

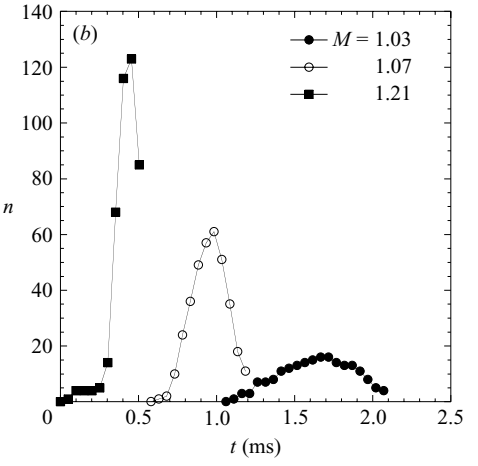


FIGURE 5. (*a*) Light transmission views of bursting liquid films for three Mach numbers. From top to bottom, $M = 1.03, 1.07, 1.21$. Time increases from left to right with a time step $\Delta t = 0.05$ ms. (*b*) Time evolution of the number of holes $n(t)$ for the three Mach numbers.

When the acceleration is time dependent, the dynamics of the perturbations linearized around the base state, $f(t)$, is exactly governed by

$$\frac{\mathrm{d}^2 f}{\mathrm{d}\tilde{t}^2} = -\tilde{k}^3 \coth(\tilde{k}) \left\{ 1 - \left[1 - \left(1 - \left(\frac{\tilde{k}_c(\tilde{t})}{\tilde{k}} \right)^4 \right) \tanh^2(\tilde{k}) \right]^{1/2} \right\} f(\tilde{t}) \qquad (4.4)$$

where $\tilde{k}_c(\tilde{t}) = We^{1/4} \Delta(\tilde{t})^{1/2}$, and $We = \rho h u^2/\sigma$ is the Weber number based on the film

https://doi.org/10.1017/S0022112004002411 Published online by Cambridge University Press

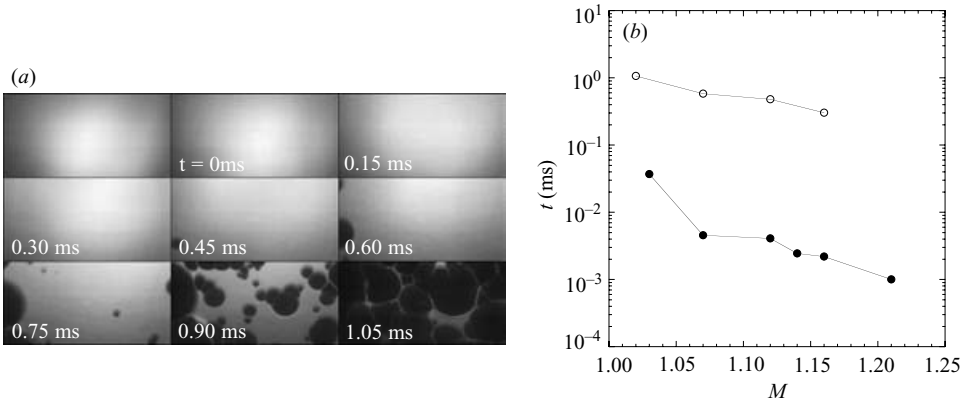


FIGURE 6. (*a*) Visualization by light reflection of the temporal film destabilization for $M = 1.07$. (*b*) Characteristic times of the instability: ●, time corresponding to the inverse of the perforation rate (t_n); ○, time of the first perforation (t_1).

velocity u and initial thickness h. At short times (i.e. for $\tilde{t} < \tilde{\tau}$), $\tilde{k}_c$ assumes a very large value and the expansion of equation (4.4) for $\tilde{k} \ll \tilde{k}_c$ is

$$\frac{\mathrm{d}^2 f}{\mathrm{d}\tilde{t}^2} = \left(\tilde{k}\tilde{k}_c^2 - \tilde{k}^2\right) f(\tilde{t}) + O\left(\frac{\tilde{k}^3}{\tilde{k}_c^2}\right). \tag{4.5}$$

The early time dynamics of the film thus coincides with that of an harmonic oscillator excited with an impulsive force proportional to $1/\tau$ and to the film velocity u. For $\tilde{t} < \tilde{\tau}$, we seek a solution to

$$\frac{\mathrm{d}^2 f}{\mathrm{d}\tilde{t}^2} + \tilde{\omega}_1^2 f(\tilde{t}) = \frac{\tilde{k} We^{1/2}}{\tilde{\tau}} \qquad \text{with} \qquad \tilde{\omega}_1 = \tilde{k} \tag{4.6}$$

of the form

$$f(\tilde{t}) = c_1 + c_2 \cos\tilde{\omega}_1\tilde{t} + c_3 \sin\tilde{\omega}_1\tilde{t}. \tag{4.7}$$

Putting (4.7) into (4.6) and using the initial conditions (4.3), we obtain

$$f(\tilde{t}) = \cos\tilde{\omega}_1\tilde{t} + \frac{\tilde{k} We^{1/2}}{\tilde{\tau}\tilde{\omega}_1^2}(1 - \cos\tilde{\omega}_1\tilde{t}) \qquad \text{for} \qquad \tilde{t} < \tilde{\tau}. \tag{4.8}$$

For times larger than $\tilde{\tau}$, the acceleration is zero and therefore $\tilde{k}_c = 0$. The expansion of equation (4.4) at small k is

$$\frac{\mathrm{d}^2 f}{\mathrm{d}\tilde{t}^2} = -\frac{\tilde{k}^4}{2} f(\tilde{t}) + O(\tilde{k}^6), \tag{4.9}$$

which is now the equation of a free harmonic oscillator with frequency $\tilde{\omega}_2 = \tilde{k}^2/\sqrt{2}$ characteristic of the peristaltic mode of the film (see § 1). We seek a solution of the form

$$f(\tilde{t}) = c_4 + c_5 \cos\tilde{\omega}_2(\tilde{t} - \tilde{\tau}) + c_6 \sin\tilde{\omega}_2(\tilde{t} - \tilde{\tau}). \tag{4.10}$$

Owing to the continuity of f and of $\mathrm{d}f/\mathrm{d}\tilde{t}$ at $\tilde{t} = \tilde{\tau}$, and expressing the impulsive character of the acceleration by letting $\tilde{\tau} \to 0$, we finally obtain

$$f(\tilde{t}) = \cos\tilde{\omega}_2\tilde{t} + \frac{\tilde{k} We^{1/2}}{\tilde{\omega}_2} \sin\tilde{\omega}_2\tilde{t} \qquad \text{with} \qquad \tilde{\omega}_2 = \frac{\tilde{k}^2}{\sqrt{2}} \tag{4.11}$$

https://doi.org/10.1017/S0022112004002411 Published online by Cambridge University Press

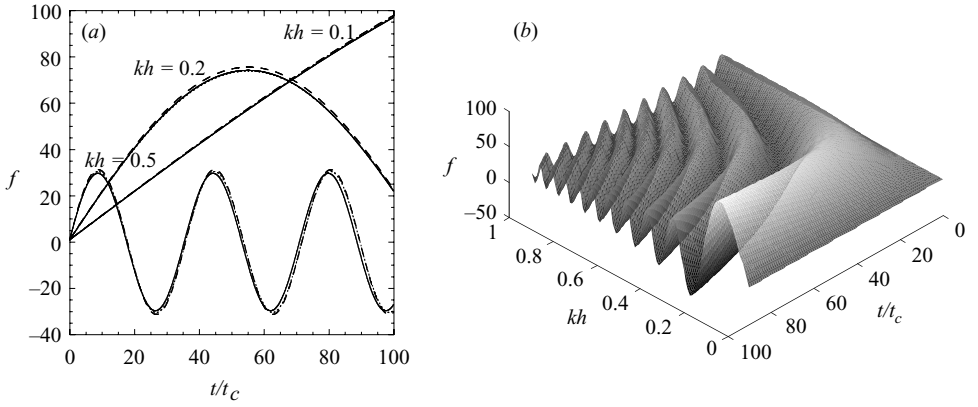


FIGURE 7. (*a*) Evolution with time of thickness modulation for three wavenumbers and for $We = 110$. The continuous line represents the result of (4.12), the discontinuous lines are the numerical solutions of (4.4) where the Dirac function is approximated by a decreasing exponential function (dashes) and a step function (dots). (*b*) Evolution of f with time and wavenumber, $We = 110$.

which describes the overall dynamics of the shape factor f. The shock excites all the wavenumbers initially, which subsequently reach the limit cycle of the varicose oscillations defined by equation (4.11) as shown on figure 7(*a*). The time it takes to reach the limit cycle decreases for increasing $\tilde{k}$ so that the most amplified wavenumber decreases as time progresses, as shown on figure 7(*b*). For $\tilde{k}^2\tilde{t} \ll 1$, relation (4.11) expands as

$$f(\tilde{t}) = 1 + We^{1/2}\tilde{k}\tilde{t} - \tfrac{1}{4}\tilde{k}^4\tilde{t}^2 + O(\tilde{k}\tilde{t}^3), \tag{4.12}$$

whose maximum at time $\tilde{t}$ such that $\partial f/\partial\tilde{t} = 0$ corresponds to the most amplified wavenumber $\tilde{k}_{\mathrm{m}}(\tilde{t})$ given by

$$\tilde{k}_{\mathrm{m}}(\tilde{t}) = We^{1/6}\tilde{t}^{-1/3}, \tag{4.13}$$

itself giving the maximal value $f_{\mathrm{m}}(\tilde{t})$ of the thickness modulations

$$f_{\mathrm{m}}(\tilde{t}) = 1 + \tfrac{3}{4}We^{2/3}\tilde{t}^{2/3}. \tag{4.14}$$

The bursting time $\tilde{t}_{\mathrm{b}}$ of the film will most likely be set when the thickness modulations are of the order of the film thickness, imposing a perforation condition $\tilde{\eta}_0 f(\tilde{t}_{\mathrm{b}}) \approx 1$ which leads to

$$\tilde{t}_{\mathrm{b}} \sim \tilde{\eta}_0^{-3/2}We^{-1}, \tag{4.15}$$

for an initial modulation $\tilde{\eta}_0$. The same condition also provides the associated wavenumber $\tilde{k}_{\mathrm{b}}$ at the burst time $\tilde{t}_{\mathrm{b}}$

$$\tilde{k}_{\mathrm{b}} \sim \tilde{\eta}_0^2We^{1/2}. \tag{4.16}$$

The thickness modulations are distributed around a most probable value. Although we do not know this distribution in detail, it is clear that the number of holes $n(\tilde{t})$ at a given time will correspond to the amplitudes on the film which have already reached the perforation criterion $\tilde{\eta}_0 f(\tilde{t}) = 1$ at time $\tilde{t}$. If $P(\tilde{\eta}_0)$ is the amplitude distribution, the relative number of perforations will be given by

$$\frac{n(\tilde{t})}{N} = \int_{\tilde{\eta}(\tilde{t})}^{1} P(\tilde{\eta}_0)\,\mathrm{d}\tilde{\eta}_0 \tag{4.17}$$

https://doi.org/10.1017/S0022112004002411 Published online by Cambridge University Press

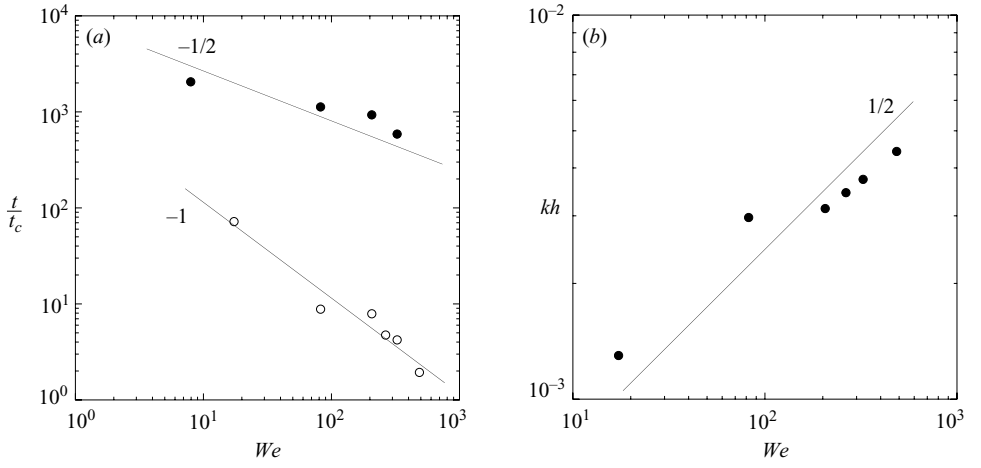


FIGURE 8. (*a*) Characteristic times of instability development as a function of the Weber number *We*: ○, $\tilde{t}_n$; ●, $\tilde{t}_1$. The film thickness is 2 μm. (*b*) Experimental selected wavenumber k_m as a function of *We*.

where N is the total number of possible holes. The instability development brings the film interfaces closer to each other at a velocity given by $\mathrm{d}f_m/\mathrm{d}\tilde{t}$ which scales as

$$\left.\frac{\mathrm{d}f_m}{\mathrm{d}\tilde{t}}\right|_{\tilde{t}_b} \sim We^{2/3}\tilde{t}_b^{-1/3} \sim We \sim \tilde{t}_b^{-1}. \tag{4.18}$$

Around its most probable value, the distribution $P(\tilde{\eta}_0)$ is flat, so that the inverse of the measured perforation rate $\tilde{t}_n$ corresponds to $\tilde{t}_b$, consistently with the observations reported on figure 8. Note that this time is representative of the modulations which have undergone the amplification and mode selection mechanism described above, and is distinct from the time of the very first perforation of the film $\tilde{t}_1$. That time relates to huge, isolated thickness modulations which perforate the film with no mode selection and, according to (4.12), scales as $We^{-1/2}$, as shown on figure 8.

A measure of the most amplified wavenumber $\tilde{k}_m(\tilde{t}_b)$ at the average burst time is provided by the maximal number of holes N recorded on the film. If the hole density is uniform on the film surface, one expects $\tilde{k}_m \sim N^{1/2} \sim We^{1/2}$, a trend consistent with that displayed on figure 8(*b*). Finally, using (4.15) and (4.16), the absolute value of the average thickness modulations is found to be $\eta_0 = 0.01$ μm for a film thickness $h = 2$ μm. This order of magnitude compares well with that measured by Krichevski & Stavans (1994) for thickness modulations solely due to thermal agitation in a comparable system.

5. Conclusion

When the thickness of an accelerated liquid film is smaller that the capillary length-scale (i.e. when $k_c h \ll 1$), the coupling of the two interfaces by the Laplace pressure rigidifies the film considerably. This is why a soap film can be inflated appreciably while keeping its interfaces locally parallel. Therefore, strong accelerations are required to initiate film destabilization in the sense of Rayleigh–Taylor. The present study uses the interaction of a shock wave with the film to achieve destabilization. The film modulates its thickness and is eventually perforated by several holes, subsequently growing in radius and connecting to each other. The initially connex liquid film results

https://doi.org/10.1017/S0022112004002411 Published online by Cambridge University Press

in a web of liquid ligaments which fragment into droplets. The film bursting time and hole density follow from a linear stability analysis with impulsive acceleration. The relatively thick films ($>1\,\mu$m) studied here have lead us to neglect van der Waals forces, as well as viscous corrections in the instability dynamics. These findings may have a more general interest in atomization processes involving liquid sheets. Such sheets often undergo a flapping motion (Villermaux & Clanet 2002) conferring on the liquid transverse accelerations which might, therefore, modulate the liquid thickness and thus initiate the breakup. This, together with the droplet size distribution coming from the disintegration of the web of ligaments after the holes have merged, is left for future research.

We thank Lazhar Houas and Georges Jourdan for giving us access to their facility at IUSTI, for their help and hospitality. Jacky Minelli is acknowledged for efficient technical support, Paul Clavin and Sergeï Gavrilyuk for an interesting discussion. This work was supported by CNES under contract 02-0485-00.

REFERENCES

Chandrasekhar, S. 1961 *Hydrodynamic and Hydromagnetic Stability*. Dover.

Culick, F. E. C. 1960 Comments on a ruptured soap film. *J. Appl. Phys.* **31**, 1128.

Henderson, L. F. 1989 On the refraction of shock waves. *J. Fluid Mech.* **198**, 365–386.

Keller, J. B. 1983 Breaking of liquid films and threads. *Phys. Fluids* **26**, 3451–3453.

Keller, J. B. & Kolodner, I. 1954 Instability of liquid surfaces and the formation of drops. *J. Appl. Phys.* **25**, 918–921.

Krichevsky, O. & Stavans, J. 1994 Surfactant-polymer interactions in freely suspended lyotropic films. *Phys. Rev. Lett.* **73**, 696–699.

Landau, L. D. & Lifshitz, E. M. 1989 *Fluid Mechanics*. Pergamon.

Lewis, D. J. 1950 The instability of liquid surfaces when accelerated in a direction perpendicular to their plane.ii. *Proc. R. Soc. Lond.* A **202**, 81–96.

Markstein, G. H. 1957 Flow disturbances induced near a slightly wavy contact surface or flame front, traversed by a shock wave. *J. Aero. Sci.* **24**, 238–239.

Meshkov, E. E. 1969 Instability of the interface of two gases accelerated by a shock wave. *Sov. Fluid Dyn.* **4**, 101–108.

Niederhaus, C. E. & Jacobs, J. W. 2003 Experimental study of the richtmyer-meshkov instability of incompressible fluids. *J. Fluid Mech.* **485**, 243–277.

Rayleigh, Lord 1883 Investigation of the character of the equilibrium of an incompressible heavy fluid of variable density. *Proc. R. Soc. Lond.* **14**, 170–177.

Richtmyer, R. D. 1960 Taylor instability in shock acceleration of compressible fluids. *Commun. Pure Appl. Maths* **8**, 297–319.

Rightley, P. M., Vorobieff, P. & Benjamin, R. F. 1997 Evolution of a shock-accelerated thin fluid layer. *Phys. Fluids* **9**, 1770–1782.

Taylor, G. I. 1950 The instability of liquid surfaces when accelerated in a direction perpendicular to their plane.i. *Proc. R. Soc. Lond.* A **201**, 192–196.

Taylor, G. I. 1959 The dynamics of thin sheets of fluid iii. disintegration of fluid sheets. *Proc. R. Soc. Lond.* **253**, 313–321.

Villermaux, E. & Clanet, C. 2002 Life of a flapping liquid sheet. *J. Fluid Mech.* **462**, 341–363.

https://doi.org/10.1017/S0022112004002411 Published online by Cambridge University Press